Article

Journal of
Nanoscience and Nanotechnology
Vol. 21, 2816–2823, 2021
www.aspbs.com/jnn

Fine-Tuning Synthesis of Fluorescent Silver Thiolate Nanoclusters

Lorenza Suber[1,*], Luciano Pilloni[2], Kshitij Khanna[1], Giuliana Righi[3], Ludovica Primitivo[4], Martina De Angelis[4], and Daniela Caschera[5]

[1] *ISM-CNR, Area della Ricerca di Roma 1, Via Salaria km 29.300, 00015, Monterotondo Scalo, RM, Italy*
[2] *SSPT-PROMAS-MATPRO ENEA CR CASACCIA, Via Anguillarese 301, 00123, Roma, Italy*
[3] *CNR-IBPM at Department of Chemisty, Sapienza Università di Roma, p.le A. Moro 5, 00185 Roma, Italy*
[4] *Department of Chemisty, Sapienza Università di Roma, p.le A. Moro 5, 00185 Roma, Italy*
[5] *ISMN-CNR, Area della Ricerca di Roma 1, Via Salaria km 29.300, 00015 Monterotondo Scalo, RM, Italy*

Noble metal thiolate nanoclusters are a new class of nanomaterials with molecular-like properties such as high dispersibility and fluorescence in the visible and infrared spectral region, properties highly requested in biomedicine for imaging, sensing and drug delivery applications. We report on three new silver phenylethane thiolate nanoclusters, differing for slight modifications of the preparation, i.e., the reaction solvent and the thiolate quantity, producing changes in the nanocluster composition as well as in the fluorescence behavior. All samples, excited in the range 250–500 nm, emit around 400 and 700 nm differing in the emission maxima and behavior. The silver thiolate nanoclusters have been characterized by way of C, H, S elemental analyses and Thermal Gravimetric Analysis (TGA) to determine the nanocluster composition, Scanning Transmission Electron Microscopy (STEM) to investigate the nanocluster morphology and UV-Vis and fluorescence spectroscopy to study their optical properties.

Keywords: Fluorescent Silver Thiolate Nanocluster, Synthesis Silver Thiolate Nanocluster, Atomic Precise Silver Nanoparticle, Monolayer Protected Silver Nanoparticle.

1. INTRODUCTION

Recently noble metal thiolate nanoclusters, a new class of nanomaterials with properties both of condensed and molecular nature, has gain attention from the scientific community. They typically possess sizes around 3–1 nm representing the "missing link" between molecular and nanoparticle behavior [1].

Their discovery is mainly due to several year researches to decrease the size of monodisperse noble metal nanoparticles since a molecular-like behavior associated with new properties was envisaged (see below).

In order to avoid nanoparticle aggregation and coalescence phenomena, the nanoparticle surface needs to be protected. Thiolates result particularly efficient as capping agents due to the strong affinity of sulfur to gold and especially silver.

Analogous to semiconductor quantum dots containing strong quantum-size confinement, when noble metal particle sizes are smaller than the exciton Bohr radius (about 4–5 nm for CdSe) [2], the nanoparticles show a size-dependent plasmon absorption band when their conduction electrons in both ground and excited states are confined to dimensions smaller than the electron mean free path (ca. 20 nm) [3], but plasmon absorption disappears completely for nanoparticles less than 2 nm and Mie's theory no longer can be applied [4]. Interestingly, metal nanoclusters are confined to a second critical regime having sizes comparable to the Fermi wavelength of the electron (ca. 0.7 nm), which results in molecule-like properties of discrete electronic states [5–7] and size-dependent fluorescence [1, 8] (i.e., a scale function of the number of atoms within the highest occupied molecular orbital (HOMO) and the lowest unoccupied molecular orbital (LUMO)).

The semiconductor quantum dots (QDs), for example CdSe, have already become a new class of fluorescent labels [2, 9] due to their unique optical properties as well as offering potential invaluable benefits such as cancer targeting [10] and biomedical imaging [11]. However, the

*Author to whom correspondence should be addressed.

 1533-4880/2021/21/2816/008 doi:10.1166/jnn.2021.19048

heavy metals contained in QDs are toxic, making them unsuitable for *in vivo* clinical application, and may pose risks to human health as well as the environment under certain conditions [12]. In contrast to QDs, noble metal nanoclusters (NCs) are highly attractive for bio-imaging and bio-labeling applications due to their low toxicity as well as ultra fine size [13]. Recent studies have focused on their quantum electronic properties including chirality [14] photoluminescence [15] quantum behavior, single-molecule optoelectronics sensing [16] and bioassay. The increasing use of metal-containing compounds in therapy and diagnosis [17] have made possible the advance of metal nanoclusters as an alternative building block of biomedical probes using their luminescent properties [18–20]. Another important application is envisaged in semi-homogeneous catalysis where the catalyst, supported on the nanocluster, has the great advantage, respect to its, unsupported employment in homogeneous catalysis to be easily recovered and reused [21–23].

In this study, as new examples of this fascinating class of materials, we report the synthesis, morphologic and optical characterization of three new fluorescent Ag phenyl-ethane thiolate nanoclusters and show how by fine tuning a few synthesis parameters, such as the reaction solvent and the molar concentration ratio Ag: thiolate, it is possible to prepare different fluorescent Ag thiolate nanoclusters with emissions both in the visible and in the near infrared spectral region.

2. EXPERIMENTAL DETAILS

All the chemicals were commercially available and were used without purification. $AgNO_3$ (99%), $Na_2S_2O_3$ (99.5%), 1-dodecyl-bromide (97%), triethylamine (Et_3N), ethanol (96%) (EtOH), acetone and di-chloromethane were purchased from Sigma Aldrich. $NaBH_4$ (95%) and Water PLUS for HPLC were acquired from Carlo Erba.

The procedure is reported in our previous publication [24]. Usually to prepare noble metal thiolate-nanoparticles or nanoclusters, thiols (RSH) are employed; they turn to thiolates cleaving the S–H bond by reaction with the noble metal salts. Alternatively, to avoid the unpleasant thiol smell, the R-thiosulphate sodium salt ($RS_2O_3Na^+$) is first prepared by reacting (2-bromoethyl) benzene (R–Br, R = C_8H_9) with sodium thiosulphate ($Na_2S_2O_3$). By subsequent reaction of RSO_3Na^+ with $AgNO_3$, the S–SO_3 bond cleavages (cleavage of the S–SO_3 bond is fast and is observed also when the thiosulphate molecule comes into contact with a noble metal film) [25] and the RS^- thiolate ligand is formed.

Preparation of NC1. 155 mg (0.64 mmol) of the thiosulphate sodium ligand $RS_2O_3Na^+$ are stirred in 10 mL EtOH. To the clear solution is added a solution of 104 mg (0.64 mmol) $AgNO_3$ in 12 ml EtOH and 3 mL H_2O. The solution gets cloudy and a white then yellowish suspension is formed in 20 minutes. After 30 minutes stirring at 40 °C, a cloudy solution of 114 mg (5.9 mmol) $NaBH_4$ in 5 mL H_2O + 20 mL EtOH is dropwise added at 70 °C. The reaction solution turns immediately red then progressively red brown. A solution of 44 mg (0.25 mmol) ascorbic acid in 3 mL H_2O is then added. After 4 hour stirring at 70 °C, the heating is turned off and the brown suspension is left under stirring overnight. The suspension is separated from a sticky residue found attached to the flask walls. The suspension is centrifuged (7000 rpm, 10 minutes). A colorless supernatant is discarded. The precipitate is washed twice with EtOH + H_2O each time discarding the colorless supernatant. Then dichlomethane and acetone (1:1v/v) are added and the suspension centrifuged at 8500 rpm for 10 minutes. The supernatant, weakly red colored, is discarded. The precipitate is added with acetone, centrifuged and the supernatant discarded, then the residue is added with boiling dichloromethane, filtered, the suspension evaporated in rota vapor and finally the red brown residue dried under vacuum. Elemental C, H, S, analyses (w/w%): C = 16.44, H = 2.02, S = 5.57 Theoretical for Ag_{12} $(SR)_3 \cdot 2H_2O + 2H_2O$ (the sample contains H_2O as evidenced by ATR-IR spectrum and TGA, see below): C = 16.21, H = 1.98, S = 5.41. TGA analysis (see Fig. 1): a weight loss of 2% at around 60 °C is attributed to 2.

H_2O molecules not coordinated to the NC whereas the weight loss of 2% above 100 °C is attributed to 2 H_2O molecules coordinated to the NC. At 300 °C: - 28% w/w (Theoretical for $-[(SR)_3 \cdot 4H_2O]$: -27% w/w).

Preparation of NC2. 310 mg (1.24 mmol) of the thiosulphate sodium ligand $RS_2O_3Na^+$ are stirred in 24 mL EtOH. The clear solution is added with a solution of 216 mg (1.24 mmol) $AgNO_3$ in 40 mL EtOH. The solution gets cloudy and the white then yellowish suspension is warmed up to 70 °C. After 30 minutes stirring at 70 °C, a cloudy dispersion of 448 mg (11.8 mmol) $NaBH_4$ in 50 mL EtOH is dropwise added at 60 °C. The reaction solution turns immediately red then progressively red

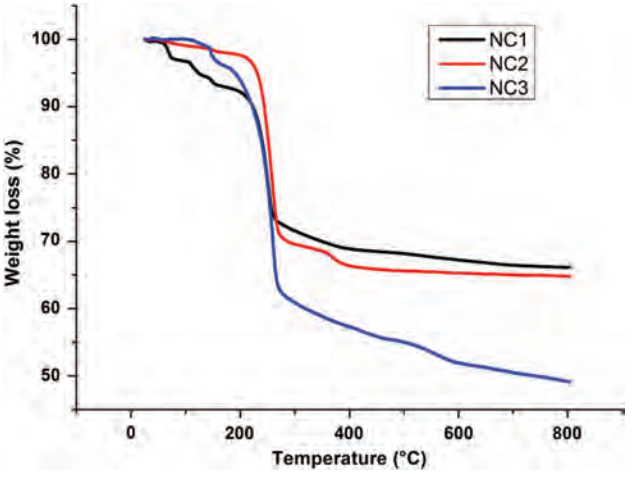

Figure 1. Thermal gravimetric analyses in argon atmosphere of NC1, NC2 and NC3 samples.

brown. A solution of 88 mg (0.5 mmol) ascorbic acid in 5 mL EtOH is then added. After 2 hour stirring at 70 °C, the heating is turned off and the brown suspension is left under stirring at room temperature for 48 hours and then heated again at 70 °C for 7 hours. The brown suspension is separated from a sticky residue found attached to the flask walls. The suspension is centrifuged (7000 rpm, 10 minutes). The colorless supernatant is discarded. The precipitate is washed twice with EtOH $+H_2O$ discarding, each time the colorless supernatant. Then dichlomethane and acetone (1:1v/v) are added and the suspension centrifuged at 8500 rpm for 10 minutes. The supernatant, weakly red colored, is discarded. The precipitate is added with acetone and centrifuged, the supernatant discarded then the residue is added with boiling dichloromethane, filtered, the dark red suspension evaporated in rota vapor and finally the red brown residue dried under vacuum.

Elemental C, H, S, analyses (w/w%): C = 24.80, H = 1.82, S = 7.52 Theoretical for $Ag_{29}(SR)_{12} \cdot EtOH$: C = 24.42, H = 2.38, S = 7.98. TGA analysis: 350 °C: −31% w/w (Theoretical for $-[(SR)_{12} \cdot EtOH]$: −31% w/w).

Preparation of NC3. 130 mg (0.525 mmol) of the thiosulphate sodium ligand $RS_2O_3Na^+$ are stirred in 5 mL EtOH. The clear solution is added with a solution of 59.45 mg (0.35 mmol) $AgNO_3$ in 10 mL hot EtOH. The solution gets cloudy and a white then yellowish suspension is formed in 20 minutes. 0.4 ml of triethyl amine are added to render basic the solution for a more efficient subsequent reduction reaction. Then 132 mg (3.5 mmol) of the reducing agent $NaBH_4$ dissolved in 10 mL hot EtOH are added. The addition is performed stepwise in five times. As soon as the first batch of the reducing agent is added, a strike change in color from lemon yellow to brown is observed. The solution darkened after the addition of last batch of reducing agent. After 2 hour heating at 70 °C, the heating is turned off and the brown suspension is left under stirring at room temperature overnight. The suspension is centrifuged (8000 rpm, 10 minutes). A cloudy white supernatant is discarded. The precipitate is washed four times with EtOH $+H_2O$. Finally the red brown residue is dried under vacuum. Elemental C, H, S, analyses (w/w%): C = 30.23, H = 2.53, S = 10.66 Theoretical for $Ag_{32}(SR)_{19} \cdot H_2O$ (the sample contains H_2O as evidenced by IR spectrum, see below): C = 30.04, H = 2.83, S = 10.02. TGA analysis: 350 °C: −42% w/w (Theoretical for $-[(SR)_{19} \cdot H2O]$: −43% w/w).

Morphologic investigation was performed by way of a Leo 1530 FE-SEM in STEM mode. A few drops of the sample dispersion in CH_2Cl_2 were deposited on a Cu grid and the solvent was let to evaporate at room temperature. The composition of the samples was investigated by way of Elemental C, H, S analyses performed using a Carlo Erba EA 1108 microanalyser at CNR-ISM. Attenuated Total Reflectance Fourier Transform Infrared (ATR-FTIR) spectra were recorded on a Shimadzu IRPrestige-21. Optical characterization was performed by way of UV-visible and fluorescence measurements. UV-visible spectra were performed on a Lambda 950 PerkinElmer spectrophotometer. Steady-state fluorescence spectra for AgNC solutions were recorded using a Fluorolog 3 (Horiba-JobinYvon) spectrofluometer, with 5 nm grids for both excitation and emission. The emissions have been collected, in the in emission and in synchronous mode, in the range 300–800 nm, exciting the sample diluted in CH_2Cl_2 with variable wavelengths from 250 to 500 nm. The corresponding excitation spectra have been collected in the range 270–600 nm, under excitation wavelengths of 500 nm and 670 nm, with 10 nm grids. All experiments were performed at room temperature using quartz cuvettes with an optical path length of 10 mm. The Raman signals of the solvent have also been collected and identified, to avoid uncorrected attributions. Suitable cut-off filters have been used to avoid Raman solvent and second harmonic signal noises. Time-resolved fluorescence measurements were carried out by a time-correlated single-photon-counting (TCSPC) system (Horiba-Jobin-Yvon). Time-resolved measurements were carried on exciting the samples using a 405 nm pulsed laser diode and collecting the emission decays around 450 nm and 670 nm, in correspondence with the two different emission signals. The fluorescence decay profiles were analyzed through decay analysis software (DAS6a HORIBA Scientific) to a multi-exponential decay equation. The quality of the fits was checked examining the residual distribution and the $\chi 2$ value.

3. RESULTS AND DISCUSSION

In the last decade several single crystal X-ray structures of noble metal thiolate nanoclusters have been solved [26–31]. The feature common to all nanoclusters is the presence of a metal (0) core and of a metal+ thiolate shell. Depending on the nature of the thiolate ligand, the metal and the reaction conditions, different metal thiolate nanocluster structures have been characterized. Nevertheless, still many efforts are devoted aiming to correlate the reaction parameters to the structures in order both to understand the formation mechanism and to optimize the reaction conditions. Unfortunately, up to now, especially for AgNCs, only few single crystal structures have been solved, the nanocluster crystallization mostly relying on a trial and error method.

The formation of Ag thiolate nanoclusters happens through an intermediate, the Ag thiolate polymeric complex $(Ag^+SR)_n$ which appears as a white/yellowish precipitate soon after the addition of the $AgNO_3$ to the ligand solution. It is this compound that reacts with the reducer $NaBH_4$ to build the AgNCs. As AgNCs are constituted both of Ag^+ ions and Ag^0 atoms, the reduction conditions are critical in determining the number of

Table I. Preparation conditions for NCs samples.

Sample	$AgNO_3$ (mM/L)	$RS_2O_3Na^+$ (mM/L)	Dispersing agent (mL)	$NaBH_4$ (mM/L)	Temperature (°C)
NC1	12.1	12.1	$EtOH + H_2O$	111.3	70
NC2	10.4	10.4	EtOH	99.1	70
NC3	14.0	21.0	EtOH	140.0	70

reduced Ag0 atoms [32]. We have modulated the reduction conditions varying the solvent, ethyl alcohol and water for NC1 and only ethyl alcohol for NC2, the difference is that the reducer $NaBH_4$ in the presence of water is more soluble and stronger than in ethyl alcohol only (Table I).

Then, with the aim to understand the influence of the ligand, we have varied the Ag:SR ratio from 1:1 (NC1) to 1:1.5 (NC3) and found that accordingly, as evidenced by the elemental analyses, in the first case the AgNC has a higher Ag:SR ratio. The composition of the NCs has been determined by elemental (C, H, S) and Thermal Gravimetric Analyses (TGA). In Figure 1 are reported the NCs thermograms performed in argon atmosphere. They show the loss of water molecules for NC1 and NC3 in the range 60–200 °C and of the thiolates above 250 °C. The Ag° w/w % content above 300–350 °C is in agreement with the one deduced from the elemental analyses results. It is to note that the composition of the nanoclusters NC2 and NC3 is known in the literature but with other thiolates, i.e., dihydrolipoic acid for NC2 [33] and glutathione for NC3 [34].

ATR-FTIR spectra of the Ag phenyl-ethane thiolate clusters NC1, NC2 and NC3 are shown in Figure 2, revealing in all samples absorptions due to solvent molecules, i.e., H_2O and EtOH in the regions around 3350 (O–H stretching vibrations), 1650 (bending O–H vibrations) and 1050 cm^{-1} (C–O absorption of EtOH for NC2).

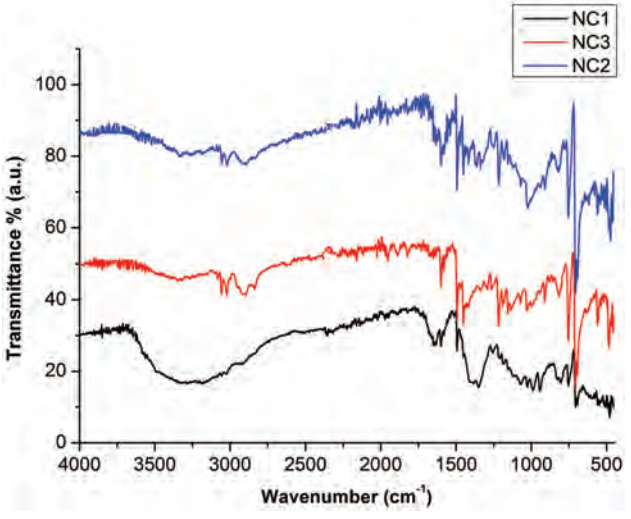

Figure 2. ATR-IR spectra of NC1, NC2 and NC3 samples.

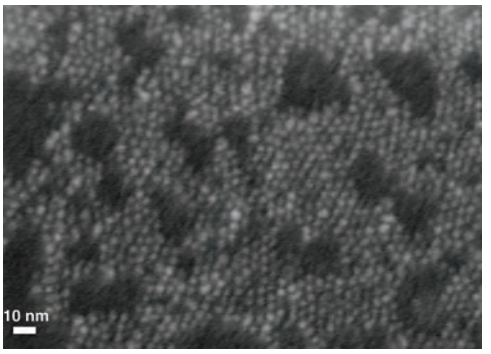

Figure 3. STEM image of 3 nm sized Ag thiolate nanoclusters (NC2 sample. The black big holes are formed during evaporation of dichlomethane solvent drops on the Cu grid sample holder).

Common to all the NCs, but better resolved in the NC2 and NC3 spectra as they have more thiolates than NC1, are three sharp bands at 3084, 3057 and 3022 cm^{-1} assigned to the stretching vibrations of the C–H groups of the phenyl ring whereas the broad absorptions centered at 2900 cm^{-1} are attributed to the stretching vibrations of the CH_2 of the ethyl group. The weak peaks between 1966 and 1824 cm^{-1} are due to overtones, the absorptions at 1602, 1496 and 1449 cm^{-1} to the stretching vibrations of C–C bonds of the aromatic ring and the strong peaks centered at 754, 708 and 695 cm^{-1} are assigned to out of plane C–H bending vibrations.

Morphologies of the Ag NCs have been investigated by STEM analysis. Figure 3 shows as an example a STEM image of AgNCs sample. The Ag thiolate nanoclusters have a size around 3 nm. They self assemble on the Cu grid during the solvent evaporation forming lamellar superstructures analogous to Ag dodecanethiolate nanoclusters [32].

AgNCs UV-Vis spectra are shown for comparison in Figure 4.

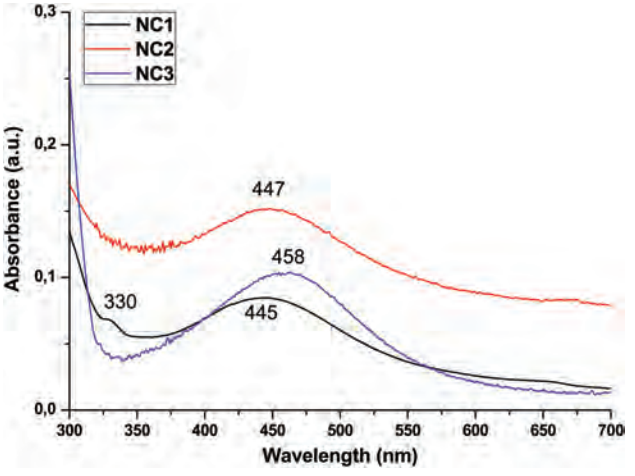

Figure 4. Comparison of UV-Vis spectra of AgNCs.

NC1 and NC2 have a very similar spectral behavior, with the maximum at about 445–448 nm, while a red shift of the maximum to higher wavelengths (458 nm) is observable for NC3. The more pronounced shift for NC3 system can be related to a stronger interaction between Ag and the thiolate ligands, due to the higher SR:Ag ratio used in the synthetic procedure. Moreover, very similar absorption features in the UV and visible region of the spectrum for Ag thiolate NCs synthesized using different thiolate ligands have already been observed [35, 36].

AgNCs are well known fluorescent systems in the NIR regions [34]. Recently it has been demonstrated that under certain conditions, also UV, blue and green emissions can be observed. In particular, the ultra-small dimensions of the nanoclusters, the nature of the Ag thiolate cage and/or strong interactions between the nanocluster's core and shell can be responsive for this behavior [32, 34, 37, 38].

Figure 5 shows the steady state fluorescence emission for NC1, excited between 300–350 nm, in synchronous mode.

Two different fluorescence signals can be observed, the first with emission at 334 and 347 nm, observed after exciting the solution up to 320 nm. The second component presents signals at 385 and 404 nm for excitation wavelengths above 330 nm. Both the components present a red shift in the emission position, dependent on the excitation wavelength. Similar emission behavior has been already observed for other Ag NCs [26, 32]. This phenomenon for small clusters may depend to equally strong transition dipole moments in the ground and excited states causing distribution of their interactions with the dielectric environment and slow mobility of this environment making the distribution persistent on a time scale emission [15]. Another suggested explanation could regard, for bigger NCs, a strong coupling between the surface plasmon and emitter [28].

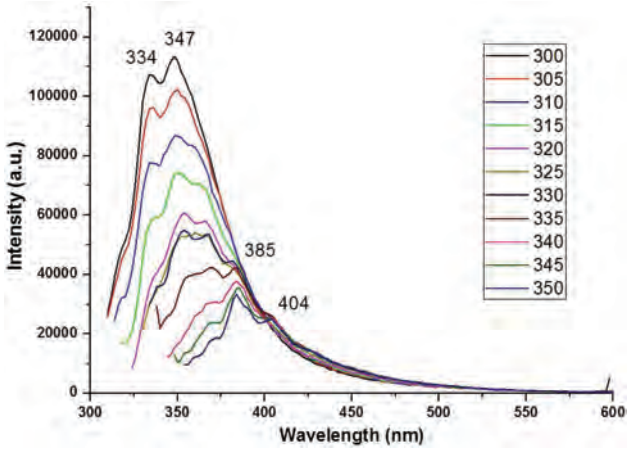

Figure 5. Steady state fluorescence emission for NC1, exciting the solution between 300 and 350 nm.

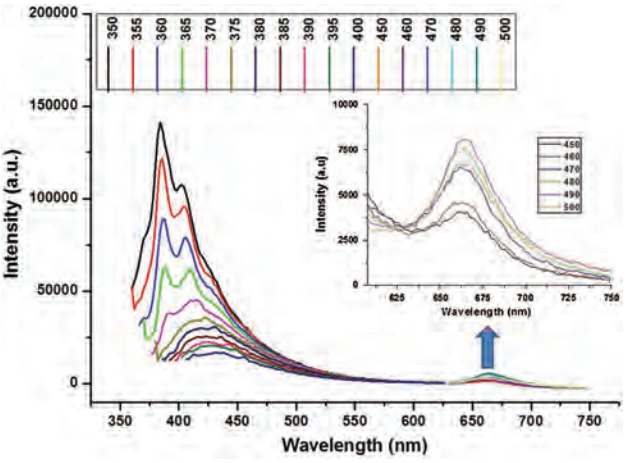

Figure 6. Steady state fluorescence emission for NC1, exciting the solution between 400 and 450 nm.

Exciting the NC1 solution above 400 nm (Fig. 6), a new emission band appears, centered at about 665 nm. This peak is independent from the excitation wavelength.

The decay times related to the two different emissions have been recorded and the results are shown in Figure 7.

Three different components have been taken into account for decay curves deconvolution, the corresponding times and relative population percent have been shown in the inset of Figure 7. The highest population percent is concentrated in the fastest decay time (0.02 ns), both for 450 and 660 nm emissions. The higher % for 450 nm could be also due to the influence of the decay of fluorescence emission under 400 nm, not detectable because of the influence of the laser prompt in the same wavelength range.

Figure 8 shows the steady state emission for NC2 at different excitation wavelengths. The steady state fluorescence behavior of NC2 is very similar to that of NC1except for a clear red shift in emission positions, both

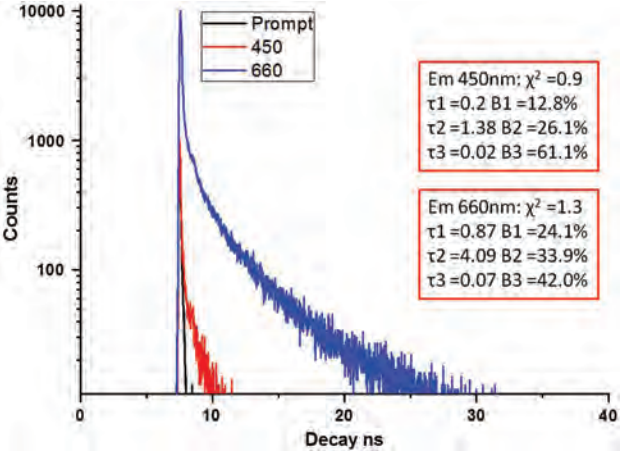

Figure 7. Comparison of time decay curves for NC1 emission at 450 nm and 660 nm. Emission at wavelengths under or near 405 nm (the laser wavelength) cannot be excited and observed in decay.

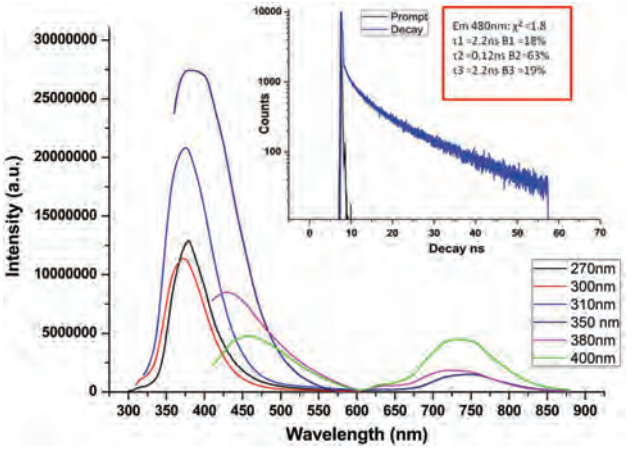

Figure 8. Steady state emission for NC2 in solution at different excitation wavelengths and time decay curve collected at 480 nm (inset). The scattering due to the second harmonic of the laser prompt is too high, at about 800 nm, to collect the relative decay time at the second emission observed in the steady state measurement.

in the UV range and in the NIR, whereas the spectral distribution is quite the same. Up to 350 nm the most evident emission peak is centered at about 375 nm, while, exciting the NC2 solution at higher wavelengths, a new emission appears at 420 nm, with a red shift strictly dependent on the excitation wavelength. Furthermore, a second broad emission, at about 730 nm can be observed for excitation above 350 nm.

On the contrary, a marked different behavior is observed for the fluorescence decay of NC2 nanocluster at 480 nm, showing a longer time decay respect to that observed for NC1 system at 450 nm ($\tau = 2.2$ ns instead of 1.38 ns), as reported in the inset of Figure 8. No information is available about the decay time at 750 nm for the NC2 system because the emission is too close to the second harmonic of laser source. The differences observed between NC1 and NC2 are to be ascribed to the different composition

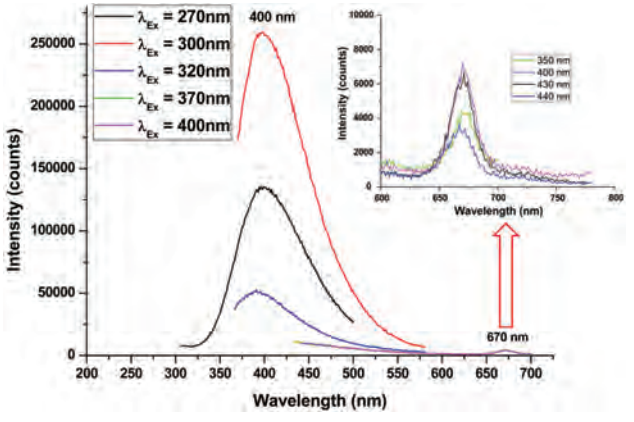

Figure 9. Fluorescence emissions for NC3 solution at different wavelength excitations. In the inset, the emission at 670 nm is shown, in the excitation range 350–450 nm.

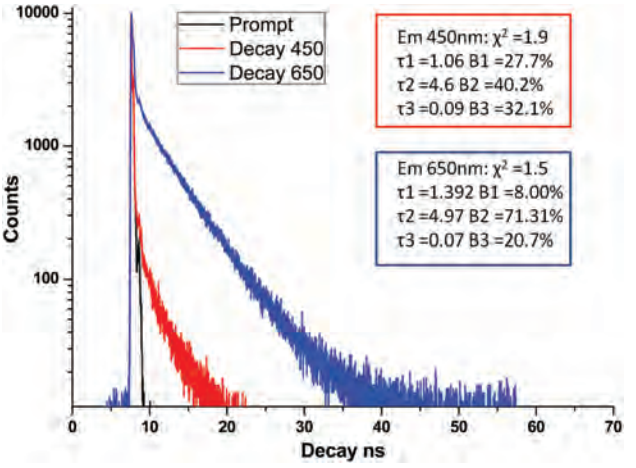

Figure 10. Comparison between the decay time curves for emissions at 450 and 650 nm for NC3 in dichlomethane solution.

and solvation as evidenced by elemental analyses and TGA measurements.

In Figure 9 it is reported the steady state fluorescence emission for NC3 solution, excited between 270–400 nm. In the UV range, a single intense emission peak can be observed, centered at about 400 nm, independently from the excitation wavelength. Also, differently from NC1 and NC2, in this case, red shifts of the UV emission peak, changing the excitation wavelength, have not been observed.

Furthermore, exciting the NC3 solutions at wavelengths above 350 nm, another emission, much lower in intensity, becomes visible at 670 nm (Fig. 9 and the corresponding inset).

The deconvolution of the decay curves, resolved using three components, is shown in Figure 10. The resulted decay times (inset Fig. 10) for the two emissions, the one at 450 nm and the other at 650 nm, are very similar, and also the fluorescence decay mechanism for this AgNC seems to be comparable with that previously observed for NC1, related to the emission at 660 nm. This clearly means that the exchange mechanism in fluorescence decay is basically the same. It is to note that also $Ag_{32}(SR)_{19}$NCs with SR = glutathione show an emission in almost the same position (660 nm) [34]. Observing the optical behavior of NC3 sample, it seems that the higher SR:Ag ratio respect to NC1 and NC2 has a stabilizing effect on the its absorption/emission mechanism.

4. CONCLUSIONS

We have demonstrated that by slight changes in the preparation conditions it is possible to isolate very different fluorescent silver thiolate nanoclusters, i.e., $Ag_{12}(SR)_3 \cdot 2H_2O$, $Ag_{29}(SR)_{12} \cdot EtOH$ and $Ag_{32}(SR)_{19} \cdot H_2O$. Steady state and time-resolved fluorescent behavior have been investigated exciting the samples diluted in CH_2Cl_2 with variable wavelengths from 250 to 500 nm. All the NCs samples show

emissions centered at around 400 and 700 nm differing in the emission maxima and behavior. More investigations, as the employment of a different laser source and ultra-fast transient absorption measurements, are planned to understand the emissions origin and optimize the systems for near-future biomedical applications.

Acknowledgments: Kshitij Khanna, undergraduate student at Institute of Chemical Technology Mumbai, completed at CNR-ISM a three-month internship (May-July 2016). The authors gratefully thank Prof. G. Ennas for TGA measurements.

References and Notes

1. Chakraborty, I. and Pradeep, T., **2017**. Atomically precise clusters of noble metals: emerging link between atoms and nanoparticles. *Chemical Reviews, 117*(12), pp.8208–8271.
2. Bruchez, M., Moronne, M., Gin, P., Weiss, S. and Alivisatos, A.P., **1998**. Semiconductor nanocrystals as fluorescent biological labels. *Science, 281*(5385), pp.2013–2016.
3. Link, S. and El-Sayed, M.A., **2003**. Optical properties and ultrafast dynamics of metallic nanocrystals. *Annual Review of Physical Chemistry, 54*(1), pp.331–366.
4. Alvarez, M.M., Khoury, J.T., Schaaff, T.G., Shafigullin, M.N., Vezmar, I. and Whetten, R.L., **1997**. Optical absorption spectra of nanocrystal gold molecules. *Journal of Physical Chemistry B, 101*(19), pp.3706–3712.
5. Apell, P., Monreal, R. and Lundqvist, S., **1988**. Photoluminescence of noble metals. *Physica Scripta, 38*(2), pp.174–179.
6. Lin, Z., Kanters, R.P.F. and Mingos, D.M.P., **1991**. Closed-shell electronic requirements for condensed clusters of the group 11 elements. *Inorganic Chemistry, 30*(1), pp.91–95.
7. Paladini, A., Catone, D., O'Keeffe, P., Toschi, F. and Suber, L., **2017**. Ultrafast depolarization of transient absorption as a probe of plasmonicity of optical transitions in Ag nanoclusters. *Plasmonics, 13*(5), pp.1687–1693.
8. Huang, C.C., Yang, Z., Lee, K.H. and Chang, H.T., **2007**. Synthesis of highly fluorescent gold nanoparticles for sensing mercury(II). *Angewandte Chemie-Int. Ed., 46*(36), pp.6824–6828.
9. Chan, W.C.W. and Nie, S., **1998**. Quantum dot bioconjugates for ultrasensitive nonisotopic detection. *Science, 281*(5385), pp.2016–2018.
10. Smith, A.M., Dave, S., Nie, S., True, L. and Gao, X., **2006**. Multicolor quantum dots for molecular diagnostics of cancer. *Expert Review of Molecular Diagnostics, 6*(2), pp.231–244.
11. Michalet, X., Pinaud, F.F., Bentolila, L.A., Tsay, J.M., Doose, S., Li, J. J., Sundaresan, G., Wu, A.M., Gambhir, S.S. and Weiss, S., **2005**. Quantum dots for live cells, in vivo imaging and diagnostics. *Science, 307*(5709), pp.538–544.
12. Hardman, R., **2006**. A toxicologic review of quantum dots: Toxicity depends on physicochemical and environmental factors. *Environmental Health Perspectives, 114*(2), pp.165–172.
13. Yahia-Ammar, A., Sierra, D., Mérola, F., Hildebrandt, N. and Le Guével, X., **2016**. Self-assembled gold nanoclusters for bright fluorescence imaging and enhanced drug delivery. *ACS Nano, 10*(2), pp.2591–2599.
14. Cathcart, N., Mistry, P., Makra, C., Pietrobon, B., Coombs, N., Jelokhani-Niaraki, M. and Kitaev, V., **2009**. Chiral thiol-stabilized silver nanoclusters with well-resolved optical transitions synthesized by a facile etching procedure in aqueous solutions. *Langmuir, 25*(10), pp.5840–5846.
15. Díez, I., Kanyuk, M.I., Demchenko, A.P., Walther, A., Jiang, H., Ikkala, O. and Ras, R.H.A., **2012**. Blue, green and red emissive silver nanoclusters formed in organic solvents. *Nanoscale, 4*(15), pp.4434–4437.
16. Chen, L.-Y., Wang, C.-W., Yuan, Z. and Chang, H.-T., **2015**. Fluorescent gold nanoclusters: Recent advances in sensing and imaging. *Analytical Chemistry, 87*(1), pp.216–229.
17. Desoize, B., **2004**. Metals and metal compounds in cancer treatment. *Anticancer Research, 24*(3A), pp.1529–1544.
18. Yuan, X., Setyawati, M.I., Tan, A.S., Ong, C.N., Leong, D.T. and Xie, J., **2013**. Highly luminescent silver nanoclusters with tunable emissions: Cyclic reduction–decomposition synthesis and antimicrobial Properties. *NPG Asia Materials, 5*(2), p.e39.
19. Zheng, K., Yuan, X., Goswami, N., Zhang, Q. and Xie, J., **2014**. Recent advances in the synthesis, characterization and biomedical applications of ultrasmall thiolated silver nanoclusters. *RSC Advances, 4*(105), pp.60581–60596.
20. Liu, J., Yu, M., Zhou, C., Yang, S., Ning, X. and Zheng, J., **2013**. Passive tumor targeting of renal-clearable luminescent gold nanoparticles: long tumor retention and fast normal tissue clearance. *Journal of American Chemical Society, 135*(13), pp.4978–4981.
21. Fang, J., Zhang, B., Yao, Q., Yang, Y., Xie, J. and Yan, N., **2016**. Recent advances in the synthesis and catalytic applications of ligand-protected, atomically precise metal nanoclusters. *Coordination Chemistry Review, 322*, pp.1–29.
22. Li, G. and Jin, R., **2013**. Atomically precise gold nanoclusters as new model catalysts. *Accounts of Chemical Research, 46*(8), pp.1749–1758.
23. Wang, Y., Wan, X.K., Ren, L., Su, H., Li, G., Malola, S., Lin, S., Tang, Z., Häkkinen, H., Teo, B.K., Wang, Q.M. and Zheng, N., **2016**. Atomically precise alkynyl-protected metal nanoclusters as a model catalyst: Observation of promoting effect of surface ligands on catalysis by metal nanoparticles. *Journal of American Chemical Society, 138*(10), pp.3278–3281.
24. Mari, A., Imperatori, P., Marchegiani, G., Pilloni, L., Mezzi, A., Kaciulis, S., Cannas, C., Meneghini, C., Mobilio, S. and Suber, L., **2010**. High yield synthesis of pure alkanethiolate-capped silver nanoparticles. *Langmuir, 26*(19), pp.15561–15566.
25. Lukkari, J., Meretoja, M., Kartio, I., Laajalehto, K., Rajamäki, M., Lindström, M. and Kankare, J., **1999**. Organic thiosulfates (bunte salts): Novel surface-active sulfur compounds for the preparation of self-assembled monolayers on gold. *Langmuir, 15*(10), pp.3529–3537.
26. Das, A., Li, T., Li, G., Nobusada, K., Zeng, C., Rosi, N.L. and Jin, R., **2014**. Crystal structure and electronic properties of a thiolate-protected Au24 nanocluster. *Nanoscale, 6*(12), pp.6458–6462.
27. Chen, Y., Zeng, C., Liu, C., Kirschbaum, K., Gayathri, C., Gil, R.R., Rosi, N.L. and Jin, R., **2015**. Crystal structure of barrel-shaped chiral $Au_{130}(p\text{-}MBT)_{50}$ nanocluster. *Journal of American Chemical Society, 137*(32), pp.10076–10079.
28. Yang, H., Lei, J., Wu, B., Wang, Y., Zhou, M., Xia, A., Zheng, L. and Zheng, N., **2013**. Crystal structure of a luminescent thiolated Ag nanocluster with an octahedral Ag6(4+) core. *Chemical Communication, 49*(3), pp.300–302.
29. Yang, H., Wang, Y. and Zheng, N., **2013**. Stabilizing subnanometer Ag(0) nanoclusters by thiolate and diphosphine ligands and their crystal structures. *Nanoscale, 5*(7), pp.2674–2677.
30. Yang, H., Wang, Y., Huang, H., Gell, L., Lehtovaara, L., Malola, S., Häkkinen, H. and Zheng, N., **2013**. All-thiol-stabilized Ag_{44} and $Au_{12}Ag_{32}$ nanoparticles with single-crystal structures. *Nature Communication, 4*(2422), pp.1–8.
31. Desireddy, A., Conn, B.E., Guo, J., Yoon, B., Barnett, R.N., Monahan, B.M., Kirschbaum, K., Griffith, W.P., Whetten, R.L., Landman, U. and Bigioni, T.P., **2013**. Ultrastable silver nanoparticles. *Nature, 501*(7467), pp.399–402.
32. Suber, L., Imperatori, P., Pilloni, L., Caschera, D., Angelini, N., Mezzi, A., Kaciulis, S., Iadecola, A., Joseph, B. and Campi, G., **2018**. Nanocluster superstructures or nanoparticles? the self-consuming scaffold decides. *Nanoscale, 10*(16), pp.7472–7483.
33. Russier-Antoine, I., Bertorelle, F., Hamouda, R., Rayane, D., Dugourd, P., Sanader, Ž., Bonačić-Koutecký, V., Brevet, P.-F. and

Antoine, R., **2016**. Tuning Ag29 nanocluster light emission from red to blue with one and two-photon excitation. *Nanoscale, 8*(5), pp.2892–2898.

34. Yau, S.H., Ashenfelter, B.A., Desireddy, A., Ashwell, A.P., Varnavski, O., Schatz, G.C., Bigioni, T.P. and Goodson, T., **2017**. Optical properties and structural relationships of the silver nanoclusters Ag 32 (SG) 19 and Ag 15 (SG) 11. *Journal of Physical Chemistry C, 121*(2), pp.1349–1361.

35. Pal, N.K. and Kryschi, C., **2015**. A facile synthesis of highly stable and luminescent Ag clusters: A steady-state and time-resolved spectroscopy study. *Physical Chemistry Chemical Physics, 17*(3), pp.1957–1965.

36. Baksi, A., Bootharaju, M.S., Chen, X., Häkkinen, H. and Pradeep, T., **2014**. Ag11(SG)7: A new cluster identified by mass spectrometry and optical spectroscopy. *Journal of Physical Chemistry C, 118*(37), pp.21722–21729.

37. Ashenfelter, B.A., Desireddy, A., Yau, S.H., Goodson, T. and Bigioni, T.P., **2015**. Fluorescence from molecular silver nanoparticles. *Journal of Physical Chemistry C, 119*(35), pp.20728–20734.

38. Jia, K., Wang, P. and Liu, X., **2015**. Facile synthesis of luminescent silver nanoparticles and fluorescence interactions with blue-emitting polyarylene ether nitrile. *Journal of Material Chemistry C, 3*(15), pp.3522–3529.

Received: 15 May 2019. Accepted: 20 January 2020.